Appl Phys B (2009) 95: 1–12
DOI 10.1007/s00340-009-3381-7

Applied Physics B
Lasers and Optics

INVITED PAPER

Filamentation "remote" sensing of chemical and biological agents/pollutants using only one femtosecond laser source

S.L. Chin · H.L. Xu · Q. Luo · F. Théberge · W. Liu · J.F. Daigle · Y. Kamali · P.T. Simard · J. Bernhardt · S.A. Hosseini · M. Sharifi · G. Méjean · A. Azarm · C. Marceau · O. Kosareva · V.P. Kandidov · N. Aközbek · A. Becker · G. Roy · P. Mathieu · J.R. Simard · M. Châteauneuf · J. Dubois

Received: 22 December 2008 / Published online: 21 February 2009

Abstract All matters in the path of filaments induced by an intense femtosecond laser pulse propagating in air could be fragmented and result in the emission of characteristic fluorescence spectra from the excited fragments. The fluorescence spectra exhibit specific signatures (fingerprints) that can be used for the identification of various substances including chemical and biological species. In this paper, we present an overview of the recent progress in our laboratory concerning the "remote" sensing of chemical and biological agents/pollutants in air using filamentation-induced nonlinear fluorescence techniques.

PACS 42.62.Fi · 42.68.Wt · 33.50.Dq

1 Introduction

In the field of laser remote sensing of chemical and biological agents/pollutants, the ideal situation would be that one laser source would do all the tasks. Conventional remote sensing techniques usually require coherent sources with a particular wavelength depending on the species to be sensed. For example, in the differential absorption LIDAR (DIAL) technique (see, e.g., [1]) the laser light has to be alternatively switched to an on-resonance wavelength, where the species under investigation absorbs, and to a neighboring off-resonance wavelength, where the species does not absorb. Although this technique has been extensively used to measure the pollutants like NO, SO_2, O_3, Hg, CH_4, and Benzene with sensitivities in the ppb range, the laser wavelengths required are over wide spectral ranges, which are

S.L. Chin · H.L. Xu (✉) · Q. Luo · F. Théberge · W. Liu · J.F. Daigle · Y. Kamali · P.T. Simard · J. Bernhardt · S.A. Hosseini · M. Sharifi · G. Méjean · A. Azarm · C. Marceau
Centre d'Optique, Photonique et Laser (COPL) & Département de Physique, de Génie Physique et d'Optique, Université Laval, Québec, G1V 0A6, Canada
e-mail: hlxu@chem.s.u-tokyo.ac.jp
Fax: +81-3-58024534

S.L. Chin
e-mail: slchin@phy.ulaval.ca
Fax: +1-418-6562623

H.L. Xu
Department of Chemistry, University of Tokyo, Tokyo 113-0033, Japan

F. Théberge · G. Roy · P. Mathieu · J.R. Simard · M. Châteauneuf · J. Dubois
Defence R&D Canada-Valcartier, Québec, G3J 1X5, Canada

W. Liu
Institute of Modern Optics, Nankai University, Key Laboratory of Opto-electronic Information Science and Technology, Education Ministry of China, Tianjin 300071, People's Republic of China

G. Méjean
Laboratoire de Spectrométrie Physique, Université J. Fourier de Grenoble, Grenoble, France

O. Kosareva · V.P. Kandidov
International Laser Center, Department of Physics, Moscow State University, Moscow, Russia

N. Aközbek
Charles M. Bowden Research Center, AMSRD-AMR-WS-ST, Redstone Arsenal, 35898 AL, USA

A. Becker
Department of Physics and JILA, University of Colorado, Boulder, CO 80303-0440, USA

not achievable by only one laser source. In particular, for biological agent detection, the UV laser-induced fluorescence LIDAR technique is usually used, where broadband spectra are generated [2, 3]. However, such broad-band fluorescence represents a weakness insofar as efficient and effective identification of biomolecules is concerned.

Recent advances in high-power femtosecond laser technologies have made it possible to examine the feasibility of such an "ideal" case. High-peak-power femtosecond laser pulses with pulse width less than 50 fs are commercially available and are made relatively compact. This development opens a new research field on "remote" sensing of chemical and biological agents/pollutants in air by filamentation-induced fluorescence based on the propagation of strong femtosecond laser pulses in air. The underlying physical mechanisms of femtosecond filamentation in transparent media are now basically understood, for which the reader is referred to several excellent review papers [4–7]. The propagation of femtosecond laser pulses in air is dominated by the dynamic equilibrium between the Kerr effect which focuses the beam and the creation of plasma which defocuses the beam. It results in the formation of self-guided structures of 100 μm in diameter called filaments. Such filamentation can be controlled to occur at a distance as far as a few kilometers in the atmosphere [8]. It is worth stressing that the filamentation can even be formed at a far distance in an adverse atmospheric environment [9] and the filaments are hardly disturbed by turbulence [10]. Inside the filament, the peak intensity is clamped to around 5×10^{13} W/cm^2 [11–13]. It is high enough to dissociate/ionize gas molecules, to explode fine particles (dusts and aerosols), and to induce "partial" breakdown on solid targets. It was predicted by one of the authors [14] that the interaction of the strong field inside the filament in air with molecules would result in "clean" fluorescence emissions practically free of plasma continuum. It was further proved that such clean fluorescence is a universal strong-field phenomenon inside the filament for all targets ranging from gases, aerosols to solids. In some cases, such as solid targets, a time-resolved technique could be used to facilitate the detection of clean fluorescence by triggering the detector properly. Furthermore, such clean fluorescence is unique from agent to agent; i.e., each agent will result in its own fingerprint fluorescence spectral characteristics. The first clean fluorescence from fragments of fluorocarbons was measured in a cell using femtosecond Ti–sapphire laser pulses [15].

Such properties of the filaments make them a promising technique with high potential in a view of applications in remote sensing of trace chemical and biological agents and pollutants in the atmosphere. In this paper, we present an overview of the recent progress in our state-of-the-art ultrafast intense laser laboratory concerning remote sensing of chemical and biological agents/pollutants in air using filamentation-induced fluorescence techniques. All experiments were carried out using the Ti–sapphire laser system generating pulses of 800 nm of 45 fs at two typical repetition rates: 1 kHz (up to 2 mJ/pulse) and 10 Hz (up to 100 mJ/pulse). We shall first discuss some physical properties and the challenge of projecting filaments to long distances in air. This is followed by a comprehensive report of the universal feasibility to remotely detect chemical and biological agents over long distances using only one laser source.

2 Physical considerations

It has been noted that the background energy (also called energy reservoir) plays a key role in the filamentation process of ultrashort strong laser pulses over long distances [16–23]. As first proposed in [16], the constant high–intensity core of a filament sustains over long distances due to the low intensity part (energy reservoir) surrounding and refilling the hot core (replenishment). Therefore, although particles, such as water droplets, snow crystals, pollens, soot, and dusts, in atmospheric air may have dimensions comparable with or larger than the filament diameters, they do not affect very much the filament propagation [24–26]. On the other hand, it was discovered that removing the background energy will lead to the termination of the filament [22, 23, 27]. In this respect, the core filament and surrounding spatial extend are not separable from each other. In [23] it was shown that after blocking the energy reservoir by an aluminum foil the filamentation process, observed via fluorescence emission from the plasma column, was terminated immediately after the pinhole. Moreover, the large spatial extent and the effect of the energy reservoir by inserting pinholes of different sizes in the filament path were discussed both experimentally and theoretically [22]. The authors observed different stages of development ranging from the termination of the filament, through its partial survival, to undisturbed propagation. A background containing up to 90% of the pulse energy was found to be necessary to maintain the filament formation, including a first refocusing. The energy in the background is more than five times larger than that found in the filament core and for the filament formation it is more critical to avoid a diffraction of energy at the edges of the background than a collision with a (small) droplet near the center. Such filamentation properties clarify why filaments can be formed and propagate in an adverse atmospheric condition, such as rain, as compared to linear propagation of the beam.

In air, the critical power for self-focusing was measured by observing the focal shift of the laser pulses [28] to be ∼10 GW for a 42 fs laser pulse; and it gradually decreases to 5 GW for (chirped) pulse duration longer than 200 fs.

However, it was shown that in some cases [29] the filamentation would be terminated even if the laser power is higher than the critical power, which was normally considered as the only criterion to predict whether the filament will terminate. This phenomenon is ascribed to the diffraction of the laser beam by the plasma produced in the filamentation process so that the remaining self-focusing power could not overcome the divergence. This would lead to a premature termination of the filament even if the power is still higher than the critical power. Therefore, the formation and termination of the filamentation process in air are mainly dependent on the energy reservoir, the diffraction of the laser beam by the self-generated plasma and the critical power of the laser pulse.

3 Technological developments for the stabilization and enhancement of fluorescence emissions

The high peak intensity inside the filament ($\sim 5 \times 10^{13}$ W/cm^2) can dissociate/ionize gas molecules [15, 30], generate higher harmonics [31–34], induce other parametric processes [35] as well as THz radiation [36–38], and explode dust particles and aerosols or induce partial breakdown on solid targets [39, 40]. However, it was found that the nitrogen fluorescence induced by the filamentation of a large diameter ($\sim$25 mm) collimated terawatt level femtosecond laser beam fluctuates significantly on a shot-to-shot basis despite the rather stable laser pulse energy [20]. It was observed that the signal intensity distribution along the propagation path as well as the starting point of the filamentation varies randomly (see Fig. 1a). The physical origin of these fluctuations in the fluorescence signal was attributed to a competition among different filaments [41]. Multiple filamentations originate from inhomogeneous intensity distribution in the transverse cross section of the laser pulse due to either initial laser imperfections arising from the source itself or during the propagation through any nonhomogeneous optical medium, which ultimately lead to the formation of multiple filaments that are copropagating in air [41–45]. Therefore, it is of particular importance to develop techniques to stabilize and to enhance the fluorescence signals induced by filamentation. In that way, it is necessary to control filamentation at a designated distance.

The effects of the initial laser beam diameter on the fluorescence signals from nitrogen molecules in air by keeping the input laser pulse energy constant was discussed in [20]. It was demonstrated that by reducing the initial beam diameter, the detected back-scattered nitrogen fluorescence from the filaments becomes much more stable on a shot-to-shot basis (Fig. 1b). In addition, it was observed that, when the beam diameter was decreased from 25 to 8 mm, the measured backscattered fluorescence signal was enhanced by three orders of magnitude. Numerical simulations were performed for a set of random initial pulse distributions imitating laser shots in both the large- and the small-beam cases [21]. In the small beam there is a faster growth of multiple filaments with propagation distance, a larger average diameter of plasma channels, and a larger overall amount of electrons in the transverse beam section. In addition, statistical processing of the simulation results showed that in the case of the small beam the number of filaments, the diameter of the plasma, and the amount of electrons are more predictable from one laser shot to another, since the ratio of $\Delta N/N$ is less significant for the small-sized beam, where N is the number of filaments and ΔN is the standard deviation of the calculated number of filaments, i.e., the error bar. These effects are associated with beam squeezing. The increase of the signal and its stability is due to the more effective usage of the background energy in the small beam. However, by decreasing the laser beam diameter, the fila-

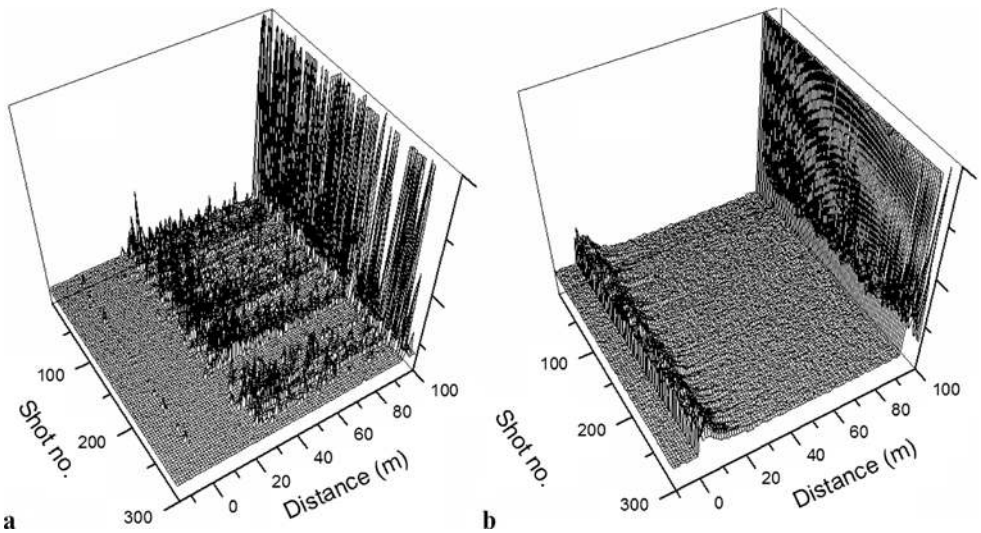

Fig. 1 Shot-to-shot backscattered fluorescence waveforms for N_2 at 337 nm detected by a photomultiplier tube. The laser energy was fixed at 30 mJ/pulse. The diameters of the beams are (**a**) 25 and (**b**) 8 mm, respectively

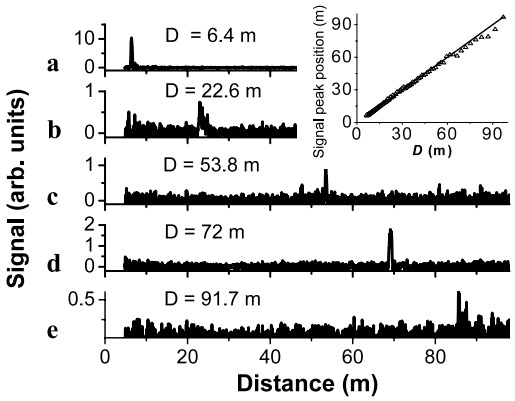

Fig. 2 LIDAR collected 337 nm signals as function of the distance for different sending telescope configurations. *D* indicates the distance between the convex mirror ($f = -50$ cm) and the calculated geometrical focus position. *Inset*: comparison between the measured fluorescence peak position (*open triangles*) and the calculated geometrical focus (*solid line*: slope = 1)

mentation onset distance is rather short, which makes this technique less attractive in remote sensing applications.

Another effective and reliable method discovered to enhance the signals was the merging of the multifilaments into a geometrical focus [46]. It was found that, in a terawatt level laser pulse, the unavoidable hot spots in the beam profile will self-focus in air at a short distance. Such early self-focusing can be overcome by using a telescope, which enlarges the diameter of the beam, thus that of the hot spots. The telescope is adjusted by varying the relative distance between the divergent and convergent optical components so that its effective focal length can therefore be much shorter than the self-focusing distance of both the enlarged beam and the hot spots, leading to multifilaments merging into the geometrical focus, as shown in Fig. 2. Since in this experimental scheme filamentation starts near the geometrical focus and the beam size is small at this position, the more effective usage of the background energy in the small beam results in consistent and strong nitrogen fluorescence signals. A similar experiment has also been performed in [47].

In addition, it is possible to control the filamentation induced by femtosecond laser pulses using adaptive optics that can modify the initial divergence of the laser pulse. It was shown in [48] that a change of both the laser energy and the beam divergence angle can precisely control the beginning of filamentation. The collapse distance increases with the beam divergence. In [49], a specially designed focusing telescope to properly deliver the laser pulses over long distances and generate powerful filaments was proposed. The telescope includes a deformable mirror that corrects the wavefront's aberrations working in a closed loop system with a wavefront sensor. This technique could be particularly useful for propagation in a turbulent atmospheric condition where the induced pulses' distortions could be compensated by the adaptive optic system. Using this configuration strong nitrogen signal was generated at a distance as far as 90 m using 40 mJ laser pulses [49]. In [50], a simple method that can generate longer filaments with higher ionization density in air was introduced. By controlling the laser beam diameter using an aperture, a significant increase in the fluorescence signal (approximately by a factor of five depending on the conditions) and an increased filament length was observed by analyzing the backscattered N_2 fluorescence collected by a LIDAR. Theoretical 3D + time stochastic numerical simulations showed that the optimum aperture size corresponds to the case where multiple filaments concentrate around the propagation axis to interfere and form a regularized elongated structure with higher overall amount of plasma.

In atmospheric remote sensing, it is of particular importance to increase the signal-to-noise ratio. For the detection of pollutants using the filamentation-induced fluorescence technique, a major noise source is the white light laser [18] generated during the filamentation process by self-phase modulation and self-steepening of the laser pulses [51–57]. This white light spectrum can span from the ultraviolet (UV) to the infrared (IR) (supercontinuum) [53, 58–61]. Although the supercontinuum provides an opportunity for atmospheric analysis by detecting the white-light absorption spectrum of pollutants [62, 63], for the filamentation-induced fluorescence technique, the white light may mask the fluorescence signals generated by the pollutant being targeted. Therefore, there is always a question whether the fluorescence from molecules can be distinguished from the backscattered supercontinuum. To answer this question, we have shown experimentally the capability of distinguishing the nitrogen fluorescence spectrum emitted from inside the filament from the backscattered supercontinuum both spectrally and over a long range in atmospheric air [64]. The spectral broadening of the supercontinuum develops progressively along the self-induced plasma column in air. The broad backscattered supercontinuum becomes fully developed at the end of a long plasma column; this is the result of the distance-cumulative effects of self-phase modulation and self-steepening of the fundamental laser pulse [53]. Still, the strong nitrogen fluorescence signals emitted in the backward direction from the beginning of the plasma column can be clearly observed, as shown in Fig. 3a. It can also be noted from the spectrum shown in Fig. 3a that detecting the fluorescence signals in the visible spectral range is difficult. However, as presented in [46], the white light noise can be controlled by generating strong and short filaments at a remote focus (c.f. Fig. 3b). Moreover, the characteristic fluorescence of atmospheric pollutants usually has a lifetime longer than that of nitrogen [30]. The pollutant fluorescence can therefore be isolated from the background, such as the nitrogen fluorescence and the backscattered supercontinuum, by temporal gating in the detection.

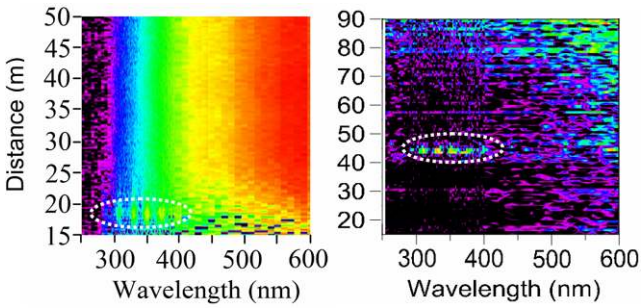

Fig. 3 Intensity distribution of the backscattered signal from 250 to 600 nm as function of the distance and the wavelength. (**a**) *Left*: using a collimated laser beam; (**b**) *Right*: using a focused beam by the telescope with $D = 45$ m. The *white dash ellipses* highlight the resolved nitrogen fluorescence

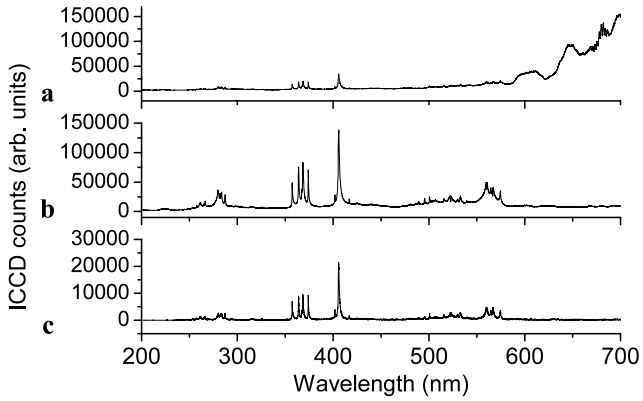

Fig. 4 Spectra of filament-induced lead plasma. The sample is located at (**a**, **c**) 4.8 and (**b**) 2.8 m away from the focal lens ($f = 5$ m). The gate widths are $t = 2$ μs (**a**, **b** and **c**) and the delay times are $\Delta t = -3$ ns (**a** and **b**) and $\Delta t = 20$ ns (**c**), respectively. Note that $t = 0$ is the laser arriving time on the target and the filament started at a distance around 2.5 m away from the focal lens

This technique considerably enhances the signal-to-noise ratio for remote detection. For solid target detections, the white light noise can be minimized by using the front part of the filaments to interact with the sample, or by means of a time-resolved measurement (Fig. 4) [65].

Moreover, in order to further increase the signal-to-noise ratio, the plasma channel left behind in the filaments was characterized in terms of the plasma density and the diameter which reflects the signal strength. In [66], it was shown using the calibrated side imaging technique that external focusing strongly influences the plasma density and the diameter of femtosecond laser filaments generated in air. The measurements of the filament showed that the average plasma density increases from 10^{15} to 2×10^{18} cm^{-3} when the focal length decreases from 380 to 10 cm while the diameter of the plasma column varies from 30 to 90 μm (the maximum at 90 μm was obtained when $f = 50$ cm). For the free propagating laser beam, an initial self-generated plasma density of 4.5×10^{14} cm^{-3} and a laser intensity of 5×10^{13} W/cm^2 inside the filament was obtained as well [66]. The femtosecond filaments in air were also characterized by using the Stark broadening analysis of the atomic oxygen fluorescence emission [67]. The electron temperature inside the plasma filament was determined to be ∼5800 K, which is relatively low compared to that in a typical nanosecond laser induced air plasma. In [65], the temperature and electron density of the plasma ejected from a lead target produced by femtosecond laser pulse filamentation in air were measured. An electron density of 8×10^{17} cm^{-3} and the plasma temperature of 6794 K were determined at a 20 ns time delay with respect to the laser pulse arriving on the target. It was shown that the continuum emission in the fluorescence spectra associated mainly with the white light due to the filamentation in ambient air can be significantly reduced by moving the starting point of the filament with respect to the target surface.

4 Detection of chemical and biological agents in air

Using the filament-induced nonlinear fluorescence technique we have remotely measured various types of samples mostly in the laboratory environment, namely, gases (CH_4, C_2H_2, and ethanol vapor) [68–70], biological agents (powders of egg white and yeast, grain dusts of barley, corn, and wheat) [71, 72], water aerosols containing multiple solutes (NaCl, $PbCl_2$, $CuCl_2$, and $FeCl_2$) [40, 73], smoke (from burning mosquito coils in air) [74], metallic targets (lead, copper, and aluminum) [65, 75, 76]. Collectively, they demonstrate the feasibility that intense femtosecond laser pulses could be applied to remote sensing of chemical and/or biologic agents. In the following, we give some representative results of the above studies.

4.1 Molecules in the gas phase

We first started by sensing methane, an atmospheric greenhouse gas, in a sealed cell [68]. Well-resolved backward fluorescence from dissociated CH radicals measured from a distance of a few meters was used to quantitatively analyze the concentration of CH_4 and its remote detection limit (Fig. 5 and the insets a–d). The estimation based on the experimental results shows that the concentration sensitivity could be down to the ppm range in the laboratory, and the detection range limit could extend up to the kilometer range with the signal at the 3σ level, where σ is the standard deviation of the noise. The fluorescence spectrum of ethanol vapor induced by the filamentation in air was also recorded using a simple telescope system [70]. In this work, ethanol was selected because it is not harmful for human health as compared to most of the hydrocarbon molecules which are toxic and unsuitable for open-air experiments in the laboratory. Backward fluorescence emission of the ethanol concentration at 0.8% could be clearly observed at a distance

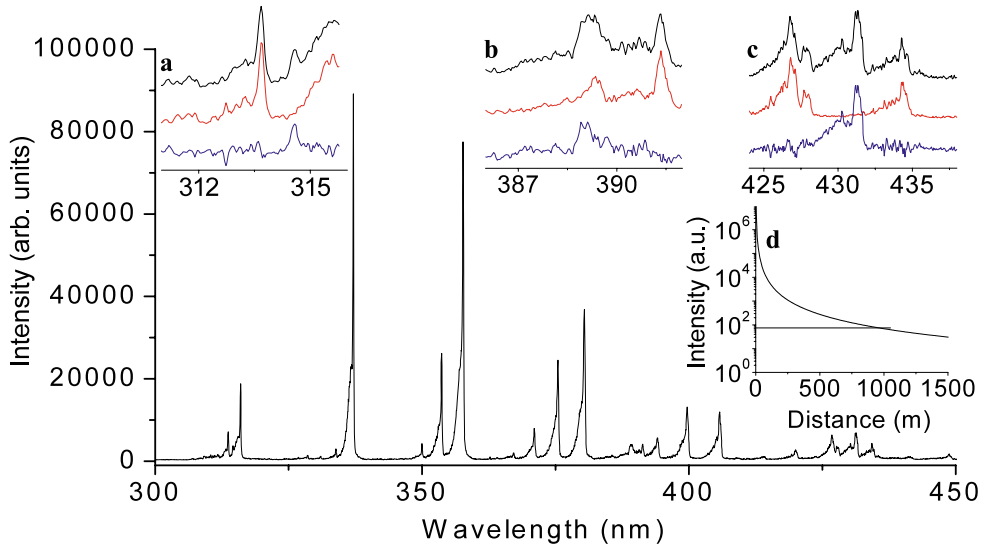

Fig. 5 Filament-induced fluorescence spectrum of a mixture of CH_4 and air with CH_4 concentration of 2.6% (volume/volume). The *insets* (**a**, **b**, and **c**) show the spectra in a higher resolution (*top*), the spectra of pure air in atmospheric pressure (*middle*), and the subtraction of the mixture and pure air spectra (*bottom*). The bands are (**a**) CH: $C^2\Sigma^+ - X^2\Pi$, (**b**) CH: $B^2\Sigma^- - X^2\Pi$, and (**c**) CH: $A^2\Delta - X^2\Pi$. The *inset* (**d**) shows the extrapolation of the detection limit according to the LIDAR equation ($I = L/R^2$, where I is the signal intensity, L is the effective filament length, and R is the distance between the end of the filament and the detector). The detection limit is about 0.9 km for the CH_4 concentration of 5% and the filament length of 20 m

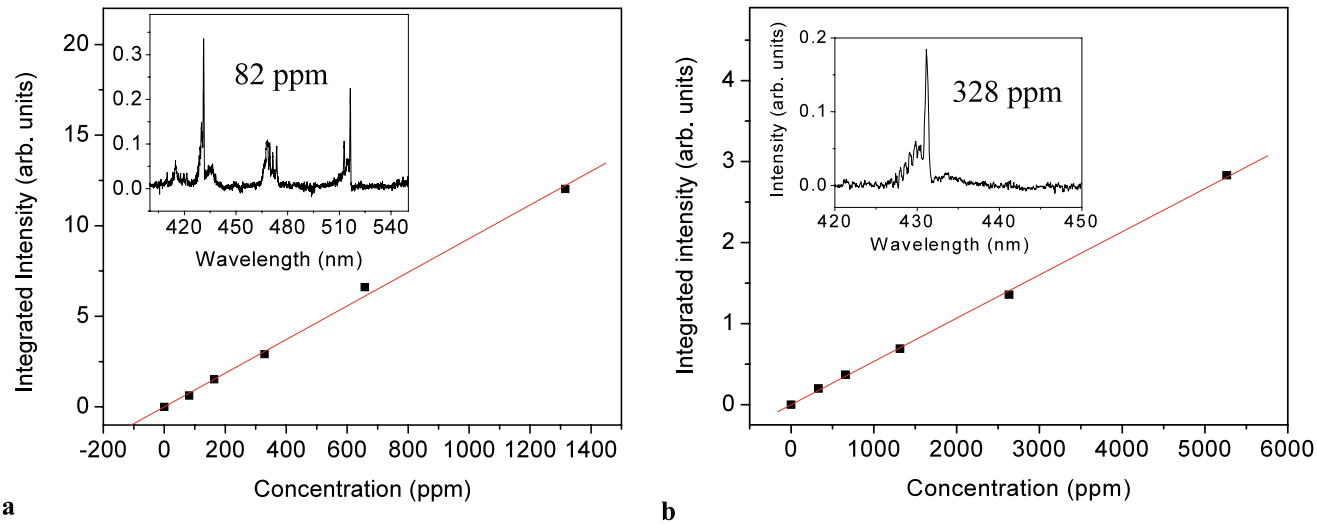

Fig. 6 Fluorescence signals (*rectangular points*) as function of (**a**) C_2H_2 and (**b**) CH_4 concentrations together with linear fits (*solid line*). The *insets* show part of the filament-induced fluorescence spectra of C_2H_2 (82 ppm) and CH_4 (328 ppm). The CH at 431 nm and the C_2 bands at 470 and 515 nm can be clearly observed. The 3σ (σ is the standard deviation of the background noise level) detection sensitivities are 350 ppb and 2 ppm for C_2H_2 and CH_4, respectively

of 30 meters. Simultaneous detection and identification of methane and acetylene mixed with air at atmospheric pressure were performed using filament-induced nonlinear spectroscopy [69]. The detection sensitivity is in the ppm–ppb concentration range depending on the induced fluorescence efficiency from the molecules (Fig. 6). In this work, a genetic algorithm was used to identify the unknown spectra with the premise that a spectral database including the spectral signatures and the strengths of the signals of the corresponding trace species is built. A good agreement between calculation and experiment for the observed species was obtained. Most recently, remote filament-induced fluorescence spectroscopy was used to probe a cloud of smoke, which was produced from burning mosquito coils located at a distance of 25 m from the laser source and LIDAR detector [74]. CN, CH, and C_2 molecular fragments were identified in the sam-

ple. It was demonstrated that the temporally gated measurement can easily suppress spectral contaminations, such as white light and atmospheric N_2 fluorescence.

The measurements mentioned above were performed only with a single near-infrared femtosecond laser, illustrating the possibility to induce characteristic fluorescence from a large number of molecular species. These results open the way to multiple species analysis in atmospheric sensing by combining filament-induced nonlinear fluorescence with suitable fluorescence collection systems.

4.2 Biological solid targets

For the detection of solid chemical–biological samples, the remarkably distinct spectra of egg white and yeast powders located 3.5 m away from the detection system was experimentally shown in [71] by using time-resolved filament-induced breakdown spectroscopy (FIBS) (Fig. 7). The same fluorescence spectrum of yeast has also been obtained successfully when the sample was located at a distance of 50 m from the laser source as well as the detection system. In particular, by using this technique, the feasibility of remote detection and differentiation of some very similar agriculture related bioaerosols, namely barley, corn, and wheat grain dusts, was also demonstrated (Fig. 8) [72]. The signals were detected in LIDAR configuration. All the species showed identical spectra, namely those from molecular C_2 and CN bands, as well as atomic Si, C, Mg, Al, Na, Ca, Mn, Fe, Sr, and K lines. These identical spectral bands and lines reveal similar chemical compositions; however, the relative intensities of the spectra are different showing different element abundances from these three biotargets. The intensity ratios of different elemental lines were used to distinguish these three samples.

4.3 Metallic targets

Filament-induced breakdown spectroscopy (FIBS) has also been applied for detecting and identifying metallic targets by Stelmaszczyk et al. [39]. Remote analysis of the copper (Cu) and iron (Fe) targets has been demonstrated at distances up to 90 m. The fluorescence spectra of the Cu target placed at a distance up to 180 m has also been presented by the same group by using femtosecond and picosecond laser pulses [77]. The advantage of FIBS for remote sensing has been explored by us by measuring the temperature and electron density of the plasma using the Stark broadening analysis of a lead target [65]. We also demonstrated that the usage of a simple telescope as sending optics could greatly improve the performance of remote FIBS (R-FIBS) of metallic targets [75]. In this case, because the filaments are short, white light continuum inside R-FIBS spectrum is negligible, realizing nongated R-FIBS, as shown in Fig. 9. Since the filaments are strong, the resulting line emission is impressively intense. The extrapolated detection limit of the aluminum sample reaches a few kilometers in distance and a few ppm in terms of minor element concentration when the sample is located 50 m away from the detection system.

Moreover, we performed a recent experiment that demonstrated the feasibility of R-FIBS of aluminum targets in an open field in a polar environment [76]. Open air visibility fluctuates with snowfall, atmospheric pressure, and relative humidity. Outside temperature was as low as −20°C. Temperature gradient from laser output to open field steps down 40°C. Under these conditions, fluorescence signals were detected in a LIDAR configuration with the aluminum target located at up to 60 m (Fig. 10). This experiment was performed using the mobile femtosecond laser facility T&T (Terawatt & Terahertz) of DRDC-Valcartier. Essentially, compared to the experiment done in the laboratory (Fig. 9), we still can distinguish the Mg impurity in the aluminum even in such adverse weather conditions.

4.4 Water aerosols containing metallic salts

Finally, R-FIBS was used for probing a cloud of microdroplets in which table salt was dissolved [73]. These microdroplets are a good simulant for aerosols. We demonstrated experimentally that R-FIBS can efficiently be used as a ppm

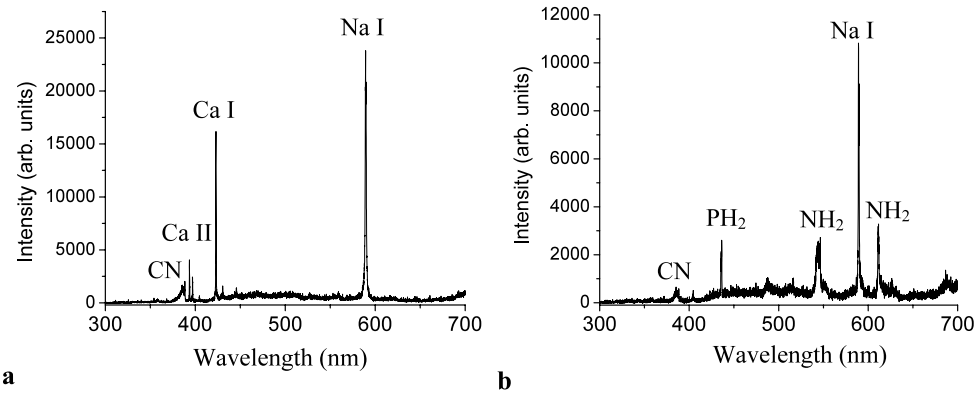

Fig. 7 Time-resolved filament-induced breakdown spectra obtained for (**a**) yeast and (**b**) egg white with the delays of $t = 10$ ns. The laser pulse energy was 7 mJ and the ICCD gate width was 500 ns

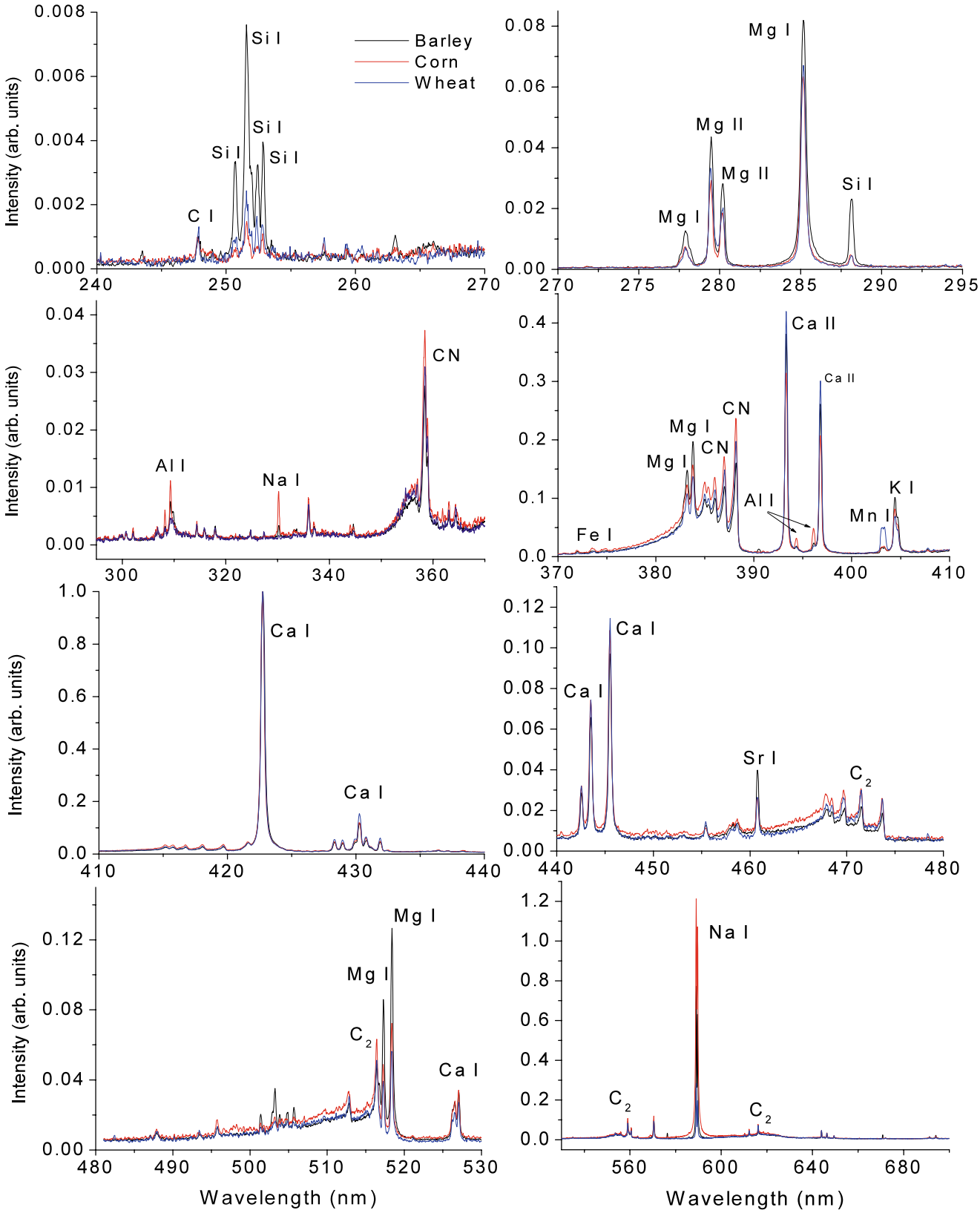

Fig. 8 Time-resolved filament-induced breakdown spectra obtained for the barley, corn, and wheat grain dusts with the delay of $t = 60$ ns with respect to the laser pulse on the target ($t = 0$). The laser pulse energy was 7 mJ and the ICCD gate width was 2 μs. The spectra are normalized to Ca I line at 422.67 nm

level sensing technique to remotely retrieve composition of microdroplets in clouds located at a distance. The technique has been successfully tested up to 70 m and, as revealed by extrapolation, showed great potential for kilometer range application. This technique is sensitive to the solvent as well. Four hydrogen bands from the Balmer series were observed in aqueous microdroplet cloud after H_2O molecules were exploded inside the filaments. Additionally, a cloud of aqueous aerosols containing a mixture of $PbCl_2$, $CuCl_2$, $FeCl_2$, and NaCl has also been detected using R-FIBS [40]. It was found that fluorescence from all the metallic ions dissolved could be observed (Fig. 11). Moreover, these spectrally narrow atomic transitions excited by the low-density plasma did not show any signal overlap.

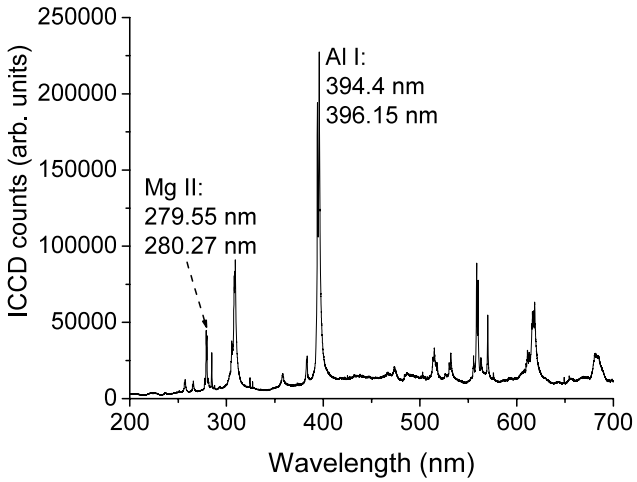

Fig. 9 Filament-induced breakdown spectrum taken for aluminum sample located 50 m away. The laser pulse energy was 108 mJ, and the ICCD gate width was 2 μs with a time delay of $t = -33$ ns with respect to the laser pulse arriving time on the target ($t = 0$)

5 Summary

In this paper, we first discussed the physics underlying the technical challenge of projecting filaments over long distances. Experimental measurements of the filament-induced characteristic fingerprint fluorescence of representative chemical and biological target examples followed. These include gases, powders, smoke, water aerosols containing multiple solutes, and metallic targets. Based on the experimental evidence, we may conclude that clean fluorescence emission of many chemical and biological targets induced by the filaments of powerful femtosecond laser pulses in air can indeed be used as the spectral fingerprint to distinguish them inside the laboratory and, through extrapolation, from a long distance of up to the kilometer range. A single laser is sufficient to induce the characteristic fluorescence for a large number of molecular species and the possibility of observing many atmospheric constituents of interest is not to be questioned anymore. This allows us to qualify the femtosecond laser filamentation as an "ideal tool" for detection and identification of atmospheric chemical and biological agents/pollutants. This opens up a new way towards remote detection of targets related to safety, security, and pollution as well as global environmental monitoring, such as green house gases.

The size of ultrafast laser sources is constantly shrinking and thus, relatively compact femtosecond remote sensing systems are possible for practical applications. However, most of the experiments presented were performed in a laboratory scale and remote sensing in the atmosphere lacks long-distance outdoor tests. Moreover, in a view of the complexity of biological matters and of fragmentary knowledge of filamentation-induced fingerprint spectra of chemical and biological agents, there are still many challenges ahead and much effort is needed to confirm the precision and reliability of this technique in the practical atmospheric measurements.

a

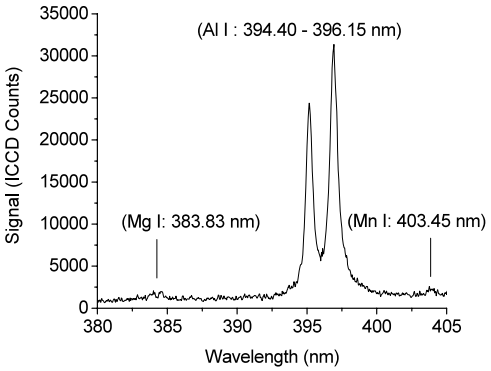

b

Fig. 10 (**a**) Outdoor field is in the center of the picture, operator and target were located at 60 m from the garage door. On the *left* is our minivan cargo and on the *right* is a warmed operator shelter. (**b**) Spectrum of Al target obtained in the winter field (Fig. 7a), where the target was located at 32 m. The laser energy and pulse duration were 225 mJ/pulse and 2 ps, respectively. Temperature was −20°C with a dew point at −22°C, and visibility was higher than nine miles

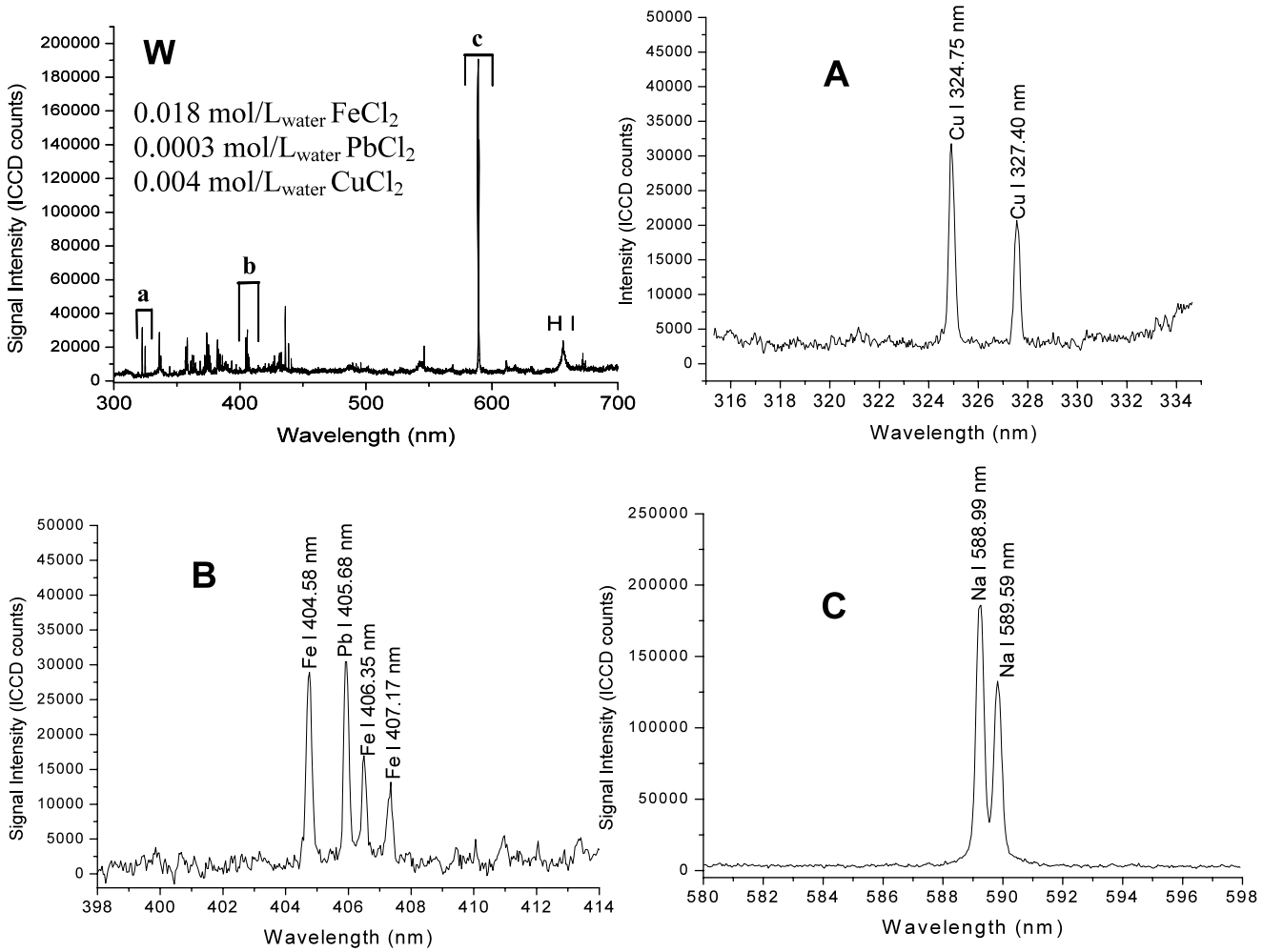

Fig. 11 Typical R-FIBS spectrum (**W**) of a thin aerosol cloud having a 95% transmission at a 632 nm wavelength and containing the listed quantities of iron dichloride, lead dichloride, copper dichloride, and sodium chloride. The regions referred to as **A**, **B**, and **C** in **W** are enlarged for clarity. **A** corresponds to Cu I atomic lines, **B** corresponds to Fe I and Pb I, and **C** corresponds to Na I

Acknowledgements We would like to thank M. Martin for the technical support. This work was supported in part by Natural Sciences and Engineering Research Council, Defence Research and Development Canada–Valcartier, Canada Foundation for Innovation, FQRNT, and Canada Research Chairs.

References

1. S. Svanberg, in *Air Pollution Monitoring with Optical Techniques*, ed. by M. Sigrist (Wiley, New York, 1994), p. 85, Chap. 3
2. R. Measures, *Laser Remote Sensing: Fundamentals and Applications* (Wiley, New York, 1988)
3. S. Svanberg, in *Laser Remote Sensing*, ed. by T. Fujii, T. Fukuchi (CRC Press, Boca Raton, 2005), p. 433, Chap. 6
4. S.L. Chin, S.A. Hosseini, W. Liu, Q. Luo, F. Théberge, N. Aközbek, A. Becker, V.P. Kandidov, O.G. Kosareva, H. Schroeder, Can. J. Phys. **83**, 863 (2005)
5. A. Couairon, A. Mysyrowicz, Phys. Rep. **441**, 47 (2007)
6. L. Bergé, S. Skupin, R. Nuter, J. Kasparian, J.-P. Wolf, Rep. Prog. Phys. **70**, 1633 (2007)
7. J. Kasparian, J.-P. Wolf, Opt. Express **16**, 466 (2008)
8. M. Rodriguez, R. Bourayou, G. Méjean, J. Kasparian, J. Yu, E. Salmon, A. Scholz, B. Stecklum, J. Eislöffel, U. Laux, P. Hatzes, R. Sauerbrey, L. Wöste, J.-P. Wolf, Phys. Rev. E **69**, 036607 (2004)
9. G. Méchain, G. Méjean, R. Ackermann, P. Rohwetter, Y.-B. André, J. Kasparian, B. Prade, K. Stelmaszczyk, J. Yu, E. Salmon, W. Winn, L.A. Schlie, A. Mysyrowicz, R. Sauerbrey, L. Wöste, J.-P. Wolf, Appl. Phys. B **80**, 785 (2005)
10. R. Ackermann, G. Méjean, J. Kasparian, J. Yu, E. Salmon, J.-P. Wolf, Opt. Lett. **31**, 86 (2006)
11. H.R. Lange, A. Chiron, J.-F. Ripoche, A. Mysyrowicz, P. Breger, P. Agostini, Phys. Rev. Lett. **81**, 1611 (1998)
12. A. Becker, N. Aközbek, K. Vijayalakshmi, E. Oral, C.M. Bowden, S.L. Chin, Appl. Phys. B **73**, 287 (2001)
13. J. Kasparian, R. Sauerbrey, S.L. Chin, Appl. Phys. B **71**, 877 (2000)
14. S.L. Chin, Method for remote sensing of pollutant molecules in a transparent medium using ultrashort intense lasers. US patent, No. US 7,184,143 B2, 27 Feb. 2007
15. J.-F. Gravel, Q. Luo, D. Boudreau, X.P. Tang, S.L. Chin, Anal. Chem. **76**, 4799 (2004)

16. M. Mlejnek, E.M. Wright, J.V. Moloney, Opt. Lett. **23**, 382 (1998)
17. M. Mlejnek, E.M. Wright, J.V. Moloney, IEEE J. Quantum Electron. **35**, 1771 (1999)
18. S.L. Chin, A. Brodeur, S. Petit, O.G. Kosareva, V.P. Kandidov, J. Nonlinear Opt. Phys. Mater. **8**, 121 (1999)
19. V.P. Kandidov, O.G. Kosareva, A.A. Koltuna, Quantum Electron. **33**, 69 (2003)
20. Q. Luo, S.A. Hosseini, W. Liu, J.-F. Gravel, O.G. Kosareva, N.A. Panov, N. Aközbek, V.P. Kandidov, G. Roy, S.L. Chin, Appl. Phys. B **80**, 35 (2005)
21. O.G. Kosareva, N.A. Panov, Akozbek, V.P. Kandidov, Q. Luo, S.A. Hosseini, W. Liu, J.-F. Gravel, G. Roy, S.L. Chin, Appl. Phys. B **82**, 111 (2006)
22. W. Liu, F. Théberge, E. Arévalo, J.F. Gravel, A. Becker, S.L. Chin, Opt. Lett. **30**, 2602 (2005)
23. W. Liu, J.-F. Gravel, F. Théberge, A. Becker, S.L. Chin, Appl. Phys. B **80**, 857 (2005)
24. F. Courvoisier, V. Boutou, J. Kasparian, E. Salmon, G. Méjean, J. Yu, J.-P. Wolf, Appl. Phys. Lett. **83**, 123 (2003)
25. A. Dubietis, E. Kucinskas, G. Tamosauskas, E. Gaizauskas, M.A. Porras, P. Di Trapani, Opt. Lett. **29**, 2893 (2004)
26. M. Kolesik, J.V. Moloney, Opt. Lett. **29**, 590 (2004)
27. O.G. Kosareva, V.P. Kandidov, A. Brodeur, C.Y. Chien, S.L. Chin, Opt. Lett. **22**, 1332 (1997)
28. W. Liu, S.L. Chin, Opt. Express **13**, 5750 (2005)
29. W. Liu, Q. Luo, F. Theberge, H.L. Xu, S.A. Hosseini, S.M. Sarifi, S.L. Chin, Appl. Phys. B **82**, 373 (2006)
30. A. Talebpour, M. Abdel-Fattah, A.D. Bandrauk, S.L. Chin, Laser Phys. **11**, 68 (2001)
31. N. Akozbek, A. Iwasaki, A. Becker, M. Scalora, S.L. Chin, C.M. Bowden, Phys. Rev. Lett. **89**, 143901 (2002)
32. N. Kortsalioudakis, M.M. Tatarakis, N. Vakakis, S.D. Moustaizis, M. Franco, B. Prade, A. Mysyrowicz, N.A. Papadogiannis, A. Couairon, S. Tzortzakis, Appl. Phys. B **80**, 211 (2005)
33. L. Berge, S. Skupin, G. Mejean, J. Kasparian, J. Yu, S. Frey, E. Salmon, J.P. Wolf, Phys. Rev. E **71**, 016602 (2005)
34. M. Kolesik, E.M. Wright, A. Becker, J.V. Moloney, Appl. Phys. B **85**, 531 (2006)
35. F. Théberge, N. Aközbek, W. Liu, A. Becker, S.L. Chin, Phys. Rev. Lett. **97**, 023904 (2006)
36. C. D'Amico, A. Houard, M. Franco, B. Prade, A. Mysyrowicz, A. Couairon, V.T. Tikhonchuk, Phys. Rev. Lett. **98**, 235002 (2007)
37. Y. Liu, A. Houard, B. Prade, S. Akturk, A. Mysyrowicz, V.T. Tikhonchuk, Phys. Rev. Lett. **99**, 135002 (2007)
38. Y. Zhang, Y. Chen, C. Marceau, W. Liu, Z.-D. Sun, S. Xu, F. Théberge, M. Châteauneuf, J. Dubois, S.L. Chin, Opt. Express **16**, 15483 (2008)
39. K. Stelmaszczyk, Ph. Rohwetter, G. Méjean, J. Yu, E. Salmon, J. Kasparian, R. Ackermann, J.P. Wolf, L. Woste, Appl. Phys. Lett. **85**, 3977 (2004)
40. J.F. Daigle, P. Mathieu, G. Roy, J.R. Simard, S.L. Chin, Opt. Commun. **278**, 147 (2007)
41. S.A. Hosseini, Q. Luo, B. Ferland, W. Liu, S.L. Chin, O.G. Kosareva, N.A. Panov, N. Aközbek, V.P. Kandidov, Phys. Rev. A **70**, 033802 (2004)
42. F. Vidal, T.W. Johnston, Phys. Rev. Lett. **77**, 1282 (1996)
43. M. Mlejnek, M. Kolesik, J.V. Moloney, E.M. Wright, Phys. Rev. Lett. **83**, 2938 (1999)
44. G. Mechain, A. Couairon, M. Franco, B. Prade, A. Mysyrowicz, Phys. Rev. Lett. **93**, 035003 (2004)
45. A. Dubietis, G. Tamosauskas, G. Fibich, B. Ilan, Opt. Lett. **29**, 1126 (2004)
46. W. Liu, F. Theberge, J.-F. Daigle, P.T. Simard, S.M. Sarifi, Y. Kamali, H.L. Xu, S.L. Chin, Appl. Phys. B **85**, 55 (2006)
47. G. Fibich, Y. Sivan, Y. Ehrlich, E. Louzon, M. Fraenkel, S. Eisenmann, Y. Katzir, A. Zigler, Opt. Express **14**, 4946 (2006)
48. Z. Jin, J. Zhang, M.H. Xu, X. Lu, Y.T. Li, Z.H. Wang, Z.Y. Wei, X.H. Yuan, W. Yu, Opt. Express **13**, 10424 (2005)
49. J.-F. Daigle, Y. Kamali, J. Bernhardt, W. Liu, C. Marceau, A. Azarm, S.L. Chin, Opt. Commun. **281**, 3327 (2008)
50. J.-F. Daigle, O. Kosareva, N. Panov, M. Bégin, F. Lessard, C. Marceau, Y. Kamali, G. Roy, V.P. Kandidov, S.L. Chin, Appl. Phys. B. doi:10.1007/s00340-008-3270-5
51. A. Brodeur, S.L. Chin, J. Opt. Soc. Am. B **16**, 637 (1999)
52. V.P. Kandidov, O.G. Kosareva, I.S. Golubtsov, W. Liu, A. Becker, N. Aközbek, C.M. Bowden, S.L. Chin, Appl. Phys. B **77**, 149 (2003)
53. N. Aközbek, M. Scalora, C.M. Bowden, S.L. Chin, Opt. Commun. **191**, 353 (2001)
54. J. Kasparian, R. Sauerbrey, D. Mondelain, S. Niedermeier, J. Yu, J.-P. Wolf, Y.-B. Andre, M. Franco, B. Prade, S. Tzortzakis, A. Mysyrowicz, M. Rodriguez, H. Wille, L. Woste, Opt. Lett. **25**, 1397 (2000)
55. G. Yang, Y. Shen, Opt. Lett. **9**, 510 (1984)
56. A.L. Gaeta, Phys. Rev. Lett. **84**, 3582 (2000)
57. M. Kolesik, G. Katona, J.V. Moloney, E.M. Wright, Appl. Phys. B **77**, 185 (2003)
58. G. Méjean, J. Kasparian, E. Salmon, J. Yu, J.-P. Wolf, R. Bourayou, R. Sauerbrey, M. Rodriguez, L. Wöste, H. Lehmann, B. Stecklum, U. Laux, J. Eislöffel, A. Scholz, A.P. Hatzes, Appl. Phys. B **77**, 357 (2003)
59. G. Méjean, J. Kasparian, J. Yu, S. Frey, E. Salmon, R. Ackermann, J.P. Wolf, L. Bergé, S. Skupin, Appl. Phys. B **82**, 341 (2006)
60. F. Théberge, W. Liu, Q. Luo, S.L. Chin, Appl. Phys. B **80**, 221 (2005)
61. F. Théberge, M. Châteauneuf, V. Ross, P. Mathieu, J. Dubois, Opt. Lett. **33**, 2515 (2008)
62. R. Bourayou, G. Méjean, J. Kasparian, M. Rodriguez, E. Salmon, J. Yu, H. Lehmann, B. Stecklum, U. Laux, J. Eislöffel, A. Scholz, A.P. Hatzes, R. Sauerbrey, L. Wöste, J.-P. Wolf, J. Opt. Soc. Am. B **22**, 369 (2005)
63. J. Kasparian, M. Rodriguez, G. Mejean, J. Yu, E. Salmon, H. Wille, R. Bourayou, S. Frey, Y.-B. Andre, A. Mysyrowicz, R. Sauerbrey, J.-P. Wolf, L. Woste, Science **301**, 61 (2003)
64. F. Théberge, W. Liu, S.A. Hosseini, Q. Luo, S.M. Sharifi, S.L. Chin, Appl. Phys. B **81**, 131 (2005)
65. H.L. Xu, J. Bernhardt, P. Mathieu, G. Roy, S.L. Chin, J. Appl. Phys. **101**, 033124 (2007)
66. F. Théberge, W. Liu, P.T. Simard, A. Becker, S.L. Chin, Phys. Rev. E **74**, 036406 (2006)
67. J. Bernhardt, W. Liu, F. Théberge, H.L. Xu, J.F. Daigle, M. Châteauneuf, J. Dubois, S.L. Chin, Opt. Commun. **281**, 1268 (2008)
68. H.L. Xu, J.F. Daigle, Q. Luo, S.L. Chin, Appl. Phys. B **82**, 655 (2006)
69. H.L. Xu, Y. Kamali, C. Marceau, P.T. Simard, W. Liu, J. Bernhardt, G. Méjean, P. Mathieu, G. Roy, J.-R. Simard, S.L. Chin, Appl. Phys. Lett. **90**, 101106 (2007)
70. Q. Luo, H.L. Xu, S.A. Hosseini, J.F. Daigle, F. Theberge, M. Sharifi, S.L. Chin, Appl. Phys. B **82**, 105 (2006)
71. H.L. Xu, W. Liu, S.L. Chin, Opt. Lett. **31**, 1540 (2006)
72. H.L. Xu, G. Méjean, W. Liu, Y. Kamali, J.F. Daigle, A. Azarm, P.T. Simard, P. Mathieu, G. Roy, J.-R. Simard, S.L. Chin, Appl. Phys. B **87**, 151 (2007)
73. J.F. Daigle, G. Méjean, W. Liu, F. Théberge, H.L. Xu, Y. Kamali, J. Bernhardt, A. Azarm, Q. Sun, P. Mathieu, G. Roy, J.R. Simard, S.L. Chin, Appl. Phys. B **87**, 749 (2007)
74. J.-F. Daigle, Y. Kamali, G. Roy, S.L. Chin, Appl. Phys. B **93**, 759 (2008)
75. W. Liu, H.L. Xu, G. Méjean, Y. Kamali, J.F. Daigle, A. Azarm, P.T. Simard, P. Mathieu, G. Roy, S.L. Chin, Spectrochim. Acta Part B **62**, 76 (2007)

76. P.T. Simard, F. Théberge, Y. Kamali, J.-F. Daigle, H.L. Xu, C. Marceau, Z.-D. Sun, J. Bernhardt, M. Châteauneuf, G. Roy, J. Dubois, S.L. Chin, internal report (2008)

77. Ph. Rohwetter, K. Stelmaszczyk, L. Wöste, R. Ackermann, G. Méjean, E. Salmon, J. Kasparian, J. Yu, J.P. Wolf, Spectrochim. Acta B **60**, 1025–1033 (2005)